RSC Advances

PAPER

View Article Online
View Journal | View Issue

Cite this: *RSC Adv.*, 2025, **15**, 7149

Application of mixed matrix hollow fiber membrane PES/B-polyphenol nanoparticle for removal of chromium hexavalent†

Yanuardi Raharjo, *[ab] Rico Ramadhan,[ac] Jourdham Nathanael,[a] Mochamad Ifan Nugroho,[a] Amelia Julia Tria Fetty[a] and Ahmad Fauzi Ismail[db]

Cr(VI) is a heavy metal with a high toxicity level. Many levels of Cr(VI) in the environment are above the established quality standards. The membrane filtration method is a technique that can be used to reduce Cr(VI) levels because it is more effective and efficient compared to other methods. In this research, the ability of a PES membrane integrated with boehmite nanoparticles coated with polyphenolic compounds from *Samanea saman* bark extract (mixed matrix hollow fiber membrane PES/B-polyphenol) was studied in reducing Cr(VI) levels. The Cr(VI) removal carried out in this research used a membrane module, so test conditions were obtained that were similar to actual conditions. XRD, FTIR, PSA, tensile strength, and SEM-EDS characterization were carried out to study the characteristics of the membrane and nanofiller. The XRD diffractogram shows a specific peak for boehmite at $2\theta = 14°$. The results of FTIR characterization of B-polyphenols also identified the presence of Al–O functional groups at wave numbers 733, 603, 474 cm^{-1} for nanofillers and OH, C=C, C–O, and C=O functional groups for PES/B-polyphenol membranes. Based on SEM-EDS and tensile strength tests, it was observed that the Young's modulus value of the membrane was 56.67 MPa and had a porous surface that was evenly distributed. Mixed matrix hollow fiber membrane PES/B-polyphenols that have been fabricated can reduce Cr(VI) levels up to 92.12%. Mixed matrix hollow fiber membrane PES/B-polyphenols have a water flux 14.1 L m^{-2} h^{-1} with porosity is 85.3% and the contact angle formed between the membrane surface and water is 58–32°. Based on the results obtained, this mixed matrix hollow fiber membrane PES/B-polyphenol has potential to be applied on a larger scale regarding its application to reduce Cr(VI) levels.

Received 26th December 2024
Accepted 26th February 2025

DOI: 10.1039/d4ra09028d

rsc.li/rsc-advances

Introduction

The presence of heavy metals is one of the main environmental issues. Heavy metals from industrial activities such as leather tanning, textiles, and electroplating can cause various problems, ranging from a decline in water quality to human health issues. Heavy metals can enter the human body through contaminated food and beverages or through air, leading to negative effects on human health.[1] The leather tanning industry is one of the industries that produce chromium (Cr) heavy metal pollution. Currently, 80–90% of leather tanning industries worldwide still use chromium as a tanning agent.[2] The leather tanning process can produce waste with chromium levels of up to 14.9 mg L^{-1}, which exceeds the tolerance limit set by the Indonesian government through the Ministry of Environment and Forestry Regulation of 0.6 mg L^{-1}. If not treated first, heavy metal content in this industrial waste will negatively impact the environmental ecosystem.

Chromium (Cr) is one of the heavy metals with carcinogenic, allergenic, and irritant properties.[3] Chromium has oxidation states, but the most stable forms in nature are trivalent chromium and hexavalent chromium.[4] Trivalent chromium has lower toxicity compared to hexavalent chromium.[5] Cr(III) in wastewater can oxidize into Cr(VI) (hexavalent chromium), a reaction that can occur spontaneously.[6] The oxidation of Cr(III) to Cr(VI) can naturally occur in soil due to photochemical oxidation or through the presence of oxidizers like MnO_2 or H_2O_2 in the soil.[7] Exposure to Cr(VI) heavy metals can lead to perforation, nasal septum damage, skin edema, asthma attacks, rhinitis, sore throat, pulmonary fibrosis, acute gastrointestinal pain, necrotic liver and kidneys, and disturbances in the stomach, urinary system, and bones.[8]

[a]*Chemistry Department, Faculty of Science and Technology, Universitas Airlangga, Surabaya 60115, Indonesia. E-mail: yanuardiraharjo@fst.unair.ac.id*

[b]*Composite Materials and Applications Research Group, Chemistry Department, Faculty of Science and Technology, Universitas Airlangga, Surabaya 60115, Indonesia*

[c]*Division of Exploration and Synthesis of Bioactive Compounds, University CoE-Research Center for Bio-Molecule Engineering, Universitas Airlangga, Jl. Dr Ir. H. Soekarno, Mulyorejo, East Java, Surabaya, 60115, Indonesia*

[d]*Advances Membrane Technology Research Centre (AMTEC), Universiti Teknologi Malaysia, Skudai, 81310, Malaysia*

† Electronic supplementary information (ESI) available. See DOI: https://doi.org/10.1039/d4ra09028d

Many methods have been developed to reduce metal ion levels in solutions. The commonly developed methods for reducing chromium levels include adsorption, bioreduction, chemical reduction, photocatalytic reduction, and electrochemical reduction.[9] Although these methods are widely used to remove Cr(VI) in wastewater, they have some drawbacks. These include requiring secondary treatment,[10] high costs for bioremediation methods,[11] the need for additional treatment to remove precipitates resulting from chemical reduction,[9] and concentration polarization that can hinder further Cr(VI) removal.[12] One material that can be used to reduce heavy metal levels is boehmite.

Boehmite is an aluminum oxide hydroxide with the chemical formula γ-AlOOH. Boehmite is commonly used as an adsorbent, particularly for separating metal ions in solutions.[13] Its high isoelectric point and point of zero charge (PZC) make boehmite highly affine and effective in adsorbing metal ions, especially Cr(VI).[14] Due to the presence of hydroxyl (–OH) groups on boehmite, it is often combined with polymer chains.[15]

The use of biomass as an adsorbent to reduce heavy metal levels has also been widely developed. The use of biosorbents is considered advantageous because the materials are natural, economical, and easy to treat. The presence of carboxyl (–COOH) and hydroxyl (–OH) groups on the surface of biomass can bind with metal ions in solution, forming chelates, thus increasing the number of active sites and enhancing the adsorbent's ability to capture metal ions.[16,17] These functional groups come from polyphenolic compounds found in plants. The use of *Samanea saman* as a biosorbent is interesting due to the abundant availability of this plant in Indonesia and the presence of polyphenolic compounds in *Samanea saman*.[18]

One drawback of using biomass adsorbents is their lower adsorption capacity compared to other inorganic material.[19] Therefore, additional methods are needed to enhance the heavy metal adsorption capacity of this biomass.

Membrane filtration is another solution for reducing heavy metal concentrations in water bodies. Membrane separation is an effective method due to its advantages, such as continuous particle separation, high permeability, and reusability.[20] Mixed Matrix Membrane (MMM) is often used to improve the function and effectiveness of membranes, especially in separating analytes from their matrix. MMM is a membrane modified by adding inorganic materials.[21,22] The efficiency of MMM increases due to the combination of adsorption and filtration methods, leading to optimal separation.[23] Fang *et al.* (2017) tested the filtration ability and fouling resistance of polyethersulfone (PES) membranes modified with polyphenolic compounds. This modification has proven to enhance the membrane's performance, particularly for water treatment applications.[24]

The novelty of this study was developed a Mixed Matrix Membrane (MMM) by combining polyethersulfone (PES) membranes with boehmite nanoparticles modified with polyphenols from *Samanea saman* bark. This combination has been proven to have the ability to remove Cr(VI) heavy metal very well. The PES was chosen because it has good oxidative, chemical properties, mechanical properties, and thermal stability.[25] The addition of boehmite–polyphenol nanofillers (B-polyphenol) is expected to improve the hydrophilicity and permeability of the fabricated membrane.[26] The membrane developed have rich in hydroxyl groups, thus increasing the ability to adsorb Cr(VI). The MMM has been casted in hollow fiber form and applied to remove Cr(VI) heavy metal ions. The hollow fiber form was chosen because it has a very large surface area, thus increasing its ability as an adsorbent.[27] The fabricated membrane will undergo performance testing to study its properties related to water treatment processes. Performance tests include water flux, porosity, hydrophilicity, and Cr(VI) removal capacity.

Experimental

Materials

The polyethersulfone (PES) (Radel A-300 Resin) and polyvinylpyrrolidone (PVP) K90 (MW: 360 000 g mol^{-1}) were purchased from Sigma-Aldrich, *N*-methylpyrrolidone (NMP) analysis grade (99.5%) was obtained from Acros Organics. Sodium hydroxide ≥ 97.0% pellets, aluminum nitrate (≥98%), 3-(chloropropyl)trimethoxysilane (≥97%), potassium dichromate (≥99.0%), and diphenylcarbazide (DPC) (≥98.0%) were purchased from Sigma-Aldrich. Meanwhile, the sulfuric acid (95.0%), acetone (≥99.5%), and ethanol (standard for GC) were obtained from Merck.

Procedure

Synthesis of boehmite–polyphenol nanoparticles (B-polyphenol). The synthesis of boehmite nanoparticles is carried out by dissolving 6.490 g of NaOH in 50 mL of deionized water, and 20 g of $Al(NO_3)_3 \cdot 9H_2O$ is dissolved in 30 mL of distilled water. The solutions are then mixed until a white solution is formed. The solution is sonicated for 3 hours at a temperature of 25 °C. The resulting mixture is placed in an oven at 220 °C for 10 hours using the hydrothermal method. The resulting precipitate is filtered, washed with deionized water, and then dried in an oven at 105 °C.[28]

The preparation of B-polyphenol begins with the extraction of polyphenols from *Samanea saman* bark powder. The extraction process starts by soaking *Samanea saman* bark powder in ethanol solvent for 2 × 24 hours. The solvent is then removed using a rotary evaporator. A total of 15 g of synthesized boehmite is added to 250 mL of ethanol/water (1 : 4 v/v) and sonicated for 15 minutes. Then, 15 mL of CPTES is added and refluxed at 50 °C for 9 hours. Afterward, 10 g of *Samanea saman* extract is added and refluxed at 60 °C for 14 hours to obtain boehmite–polyphenol nanoparticles (B-polyphenol). The B-polyphenol is separated by centrifugation, washed with ethanol, and dried in an oven at 60 °C.[29]

Preparation of dope solution. The dope of MMM was fabricated by mixing the PES, PVP, NMP, and B-polyphenol. The pellet of PES used was 18 wt%, while the PVP loading used was 1 wt%. The B-polyphenol loading was varied at 0; 0.5; 1.0; 1.5; and 2.0 wt%. The dope solution was heating at 60 °C for 6 h then continuously stirrer for 1 day.

Hollow fiber membranes fabrication. The dry/wet spinning hollow fiber machine was used to fabricate the hollow fiber membrane. The single layer spinneret with diameter size for inner and outer 0.4/0.8 mm was used in this study. The spinneret was placed by distance 40 cm with the coagulant bath. The dope extrusion rate used was 1 mL min^{-1}, bore fluid (distilled water) pumping speed was 1 mL min^{-1}, and collection speed is 5 m min^{-1}. The post-treatment of hollow fiber-MMM (HF-MMM) was washing for 50 h by tap water, thus immersion in 10 wt% glycerol for 24 h.[30]

B-polyphenol characterization

X-ray diffractometer (XRD). The boehmite and B-polyphenol were characterized by XRD to make sure the boehmite and B-polyphenol successfully synthesized. The spectra obtained by XRD (Rigaku-Ultima) were measured in the range 2θ from 5° to 90°.

Fourier-transform infrared spectroscopy (FTIR). The FTIR was measured to analysis the functional group of the boehmite and B-polyphenol studied. The ATR-FTIR (PerkinElmer Inc., USA) instrument to be analyzed in the range 4000 to 400 cm^{-1}.

Scanning electron microscopy (SEM). The SEM (Hitachi) was used obtained the structural morphology of B-polyphenol. The gold was used as sputter-coated of B-polyphenol powder before analysis.

Particle size analyzer (PSA). The PSA were used to measure the particle size of B-polyphenol and confirm that B-polyphenol has a nanoscale size.

Hollow fiber membrane characterization

Scanning electron microscopy (SEM). The structural morphology of the HF-MMM produced was observed by field-emission scanning electron microscope (TM3000, Hitachi, USA). The inner surface, outer surface, and cross-section views were observed.

Fourier-transform infrared spectroscopy (FTIR). The FTIR was measured to analysis the functional group of HF-MMM. The ATR-FTIR (PerkinElmer Inc., USA) instrument to be analyzed in the range 4000 to 400 cm^{-1}.

Water contact angle (WCA)

The contact angle of surface membranes was determined using sessile drop technique. The experiment conducted on a goniometer (Model: Kruss Gambult, Germany) which consists of a computer-controlled automatic liquid deposition system and deionized water is used in measurements. A small drop 0.3 μL of water dropped on the surface of the membrane using a syringe, three strands of membrane fibers were randomly chosen for contact angle measurement.

Porosity

Membrane porosity (ε) was measured by dry–wet weight method. The membrane fibers (10 pieces × 5 cm) were equilibrated in water for 5 hours. The membrane fibers were weighed after adsorption of the water and after dried on a filter paper. The membrane porosity was calculated by eqn (1).

$$\varepsilon = \frac{M_1 - M_2}{V \times \delta_{\text{water}}} \times 100\% \quad (1)$$

where, M_1 and M_2 are the weights of wet and dry membrane (gram), respectively. V is volume of HF membrane (cm^3) and δ_{water} is the density of pure water (g cm^{-3}).

Tensile strength test

The preparation involves fabricating the membrane in the form of a flat sheet using the same composition as for the HF membrane. Before testing, the initial length of the flat sheet membrane is measured. Then, both ends of the membrane are clamped with a tensile testing device. The sample is stretched with the tensile tester until it breaks. When the sample breaks, the monitor on the tensile tester will display the load required to break the membrane and the change in length. From the obtained data, the stress (σ) and strain (ε) values can be determined.

Membrane performance

Water flux. The water flux test is conducted using the single strand membrane test method. The test begins by measuring the surface area of the synthesized membrane. Total of 100 mL of water is passed through the membrane while recording the testing time. The permeate (the solution that passes through the membrane) is collected, and its volume is measured. The water flux value can be calculated using eqn (2). Those performance tested by using set up experiments on Fig. 1.

$$J_{\text{W}} = \frac{V}{A \times t} \quad (2)$$

where J_{W} is the flux of solute (L m^{-2} h^{-1}); J_{S} is the flux of solute (mg m^{-2} h^{-1}), V is the volume of permeate (L), A is the effective surface area (m^2), and t is the time of flux measurement (h).

Cr(VI) clearence

The primary test conducted in this research is the evaluation of the membrane's ability to reduce Cr(VI) concentration. The optimization parameters include the mass of B-polyphenol, the pH of the feed solution, and the concentration of the feed

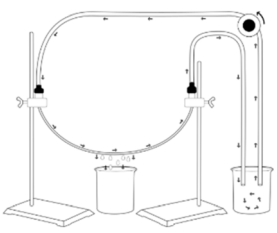

Fig. 1 Schematic experimental set-up for cross flow single hollow fiber membrane.

solution. A total of 100 mL of Cr(VI) feed solution is passed through the membrane *via* a membrane module. The permeate solution is collected and analyzed for the remaining Cr(VI) concentration. The Cr(VI) concentration in the permeate solution is referred to as the post-treatment concentration. This concentration is compared to the pre-treatment concentration, and the Cr(VI) removal efficiency is calculated using eqn (3).

$$R(\%) = \left(1 - \frac{\text{permeate concentration}}{\text{feed concentration}}\right) \times 100\% \quad (3)$$

R (%) represents the percentage removal of hexavalent chromium before and after passing through the membrane. The concentration of Cr(VI) has been analyzed by using spectrophotometer UV-vis at wavelength 540 nm with addition of DPC and acidity is adjust using H_2SO_4.

Results and discussion

Formation of B-polyphenol

The B-polyphenol was synthesized by boehmite nanoparticles (B) and polyphenol by using silane coupling agent (3-chloropropyl triethoxysilane (CPTES)). Boehmite was synthesize by several step, *i.e.* $Al(OH)_3$, alumina bayerite, alumina gibbsite, then the final step was become alumina γ-AlOOH which is in the form of a white powder according to the chemical reaction in the chemical reaction (4).

$$Al(NO_3)_3 \cdot 9H_2O_{(s)} + 3NaOH_{(aq)} \rightarrow Al(OH)_{3(s)} + 9H_2O_{(l)} + 3Na_{(aq)}^{+} + 3NO_{3(aq)}^{-}$$
$$Al(OH)_{3(s)} \rightarrow \gamma\text{-}AlOOH_{(s)} + H_2O_{(l)} \quad (4)$$

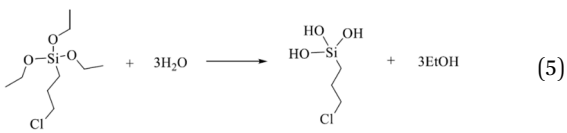

(5)

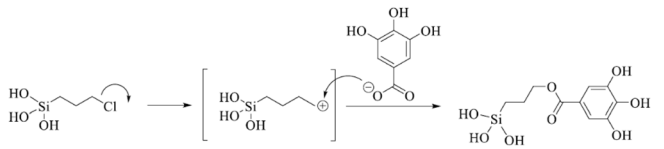

(6)

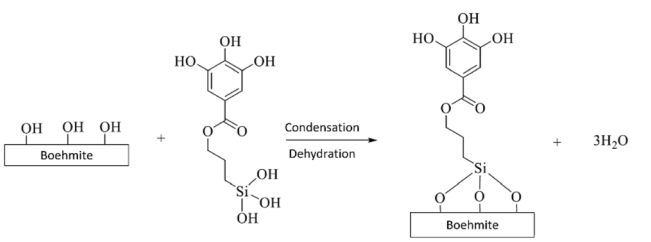

(7)

The synthesized boehmite is coated with polyphenol compounds from *Samanea saman* bark and named B-polyphenol. The purpose of coating boehmite with polyphenol is to improve the performance of the membrane, especially related to the separation ability of an analyte. The addition of polyphenol to the surface of boehmite nanoparticles can increase the hydrophilicity, water flux, and anti-fouling resistance of the fabricated membrane.[31] The addition of polyphenol also involves the presence of a silane coupling agent (3-chloropropyl triethoxysilane (CPTES)) which acts as an intermediary in the formation of bonds between organic compounds and inorganic materials. The use of silane coupling agents can also prevent agglomeration in nano materials, so that it can maximize the function and active side of nano materials in their use as membrane filler materials.[32]

The coating of boehmite by organic polyphenol compounds using CPTES occurs through several stages. The coating begins with the binding of CPTES to the nanostructure of boehmite material. At this stage, CPTES undergoes a hydrolysis process to form silanol groups.[33] Silanol groups (Si–O–H) are formed so that they can bind to boehmite nanoparticles on their surfaces which contain many –OH groups. The hydrolysis reaction of CPTES can be seen in the chemical reaction (5).

Furthermore, boehmite is immobilized by organic polyphenol compounds through the SN1 substitution mechanism.[34] Polyphenol compounds are substituted with Cl atoms in CPTES. At this stage, a bond will be formed between CPTES and organic polyphenol compounds. The substitution reaction occurs through the formation of carbocation intermediates. This stage determines the reaction rate of the binding of CPTES and polyphenols. The substitution reaction of CPTES and polyphenols can be seen in the chemical reaction (6).

The next stage is the binding of CPTES to the boehmite surface. The bonding site occurs on the boehmite surface which has many –OH groups with silanol groups on CPTES. At this stage, dehydration occurs due to the heating process that occurs. The binding reaction of CPTES and boehmite can be seen in the chemical reaction (7).

Characterization of B-polyphenol nanoparticle

The SEM image of B-polyphenol are shown in Fig. 2. The image shows the morphological observations of boehmite examined at magnifications of 2500× and 5000×. At a magnification of 2500×, the boehmite particles appear to cluster due to agglomeration. Based on observations using SEM conducted by He *et al.* (2016), boehmite is a material that tends to agglomerate.[35] The tendency of boehmite to agglomerate is also highly dependent on the temperature and concentration of the reactants used. As the concentration of the reactants increases, a negatively charged secondary layer forms on the surface of the $Al(OH)_3$ precipitate, leading to repulsion between particles and resulting in relatively smaller agglomeration sizes (<50 μm).[36]

The XRD characterization results of the synthesized boehmite and B-polyphenol can be seen in Fig. 3. Based on the peaks observed in the diffractogram, it is evident that boehmite crystals have formed. This is supported by the correspondence

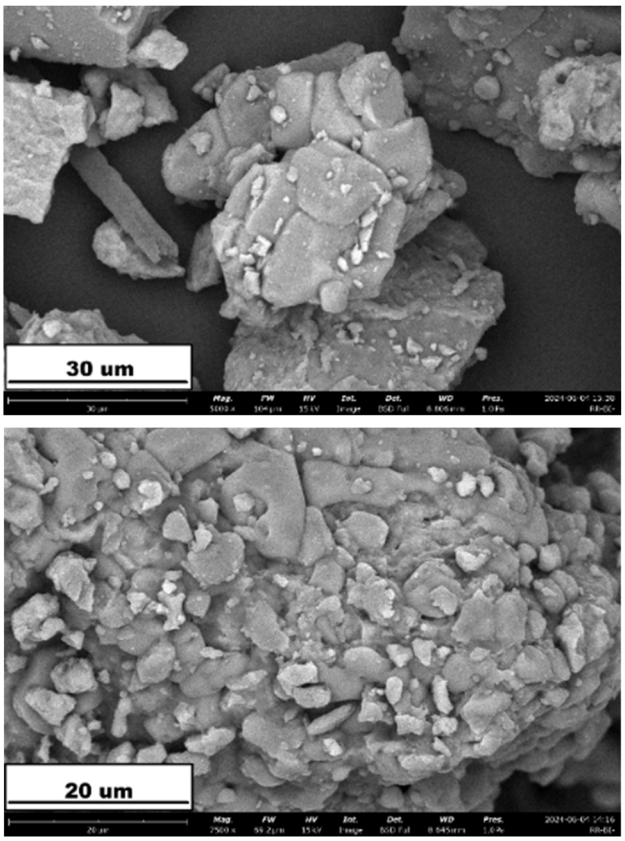

Fig. 2 SEM image of B-polyphenol.

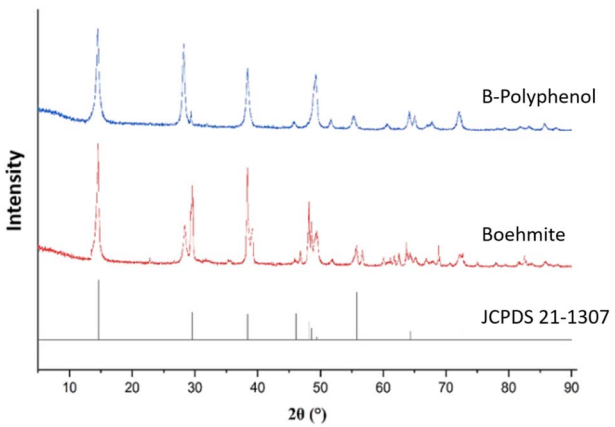

Fig. 3 XRD spectra of boehmite and B-polyphenol.

of the diffractogram peaks between the synthesized boehmite and the JCPDS data number 21-1307. In the diffractogram of the synthesized boehmite, the angle $2\theta = 14°$ is a characteristic peak of boehmite nanomaterial, indicating that the crystal structure of boehmite has been formed through the synthesis process conducted.[37] The presence of polyphenol coating on the boehmite nanomaterial can be substantiated by the results of the XRD diffractogram analysis. As shown in Fig. 3, there is a noticeable change in the intensity of the dominant crystal phase between the pure boehmite nanomaterial and B-

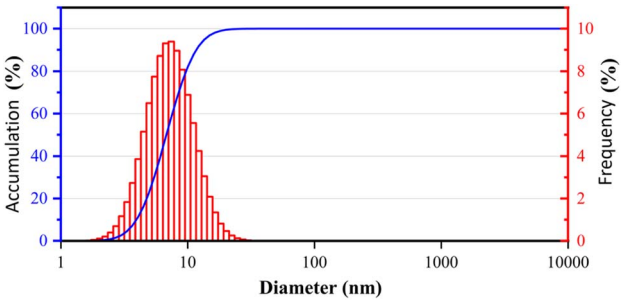

Fig. 4 The particle size distribution results of B-polyphenol.

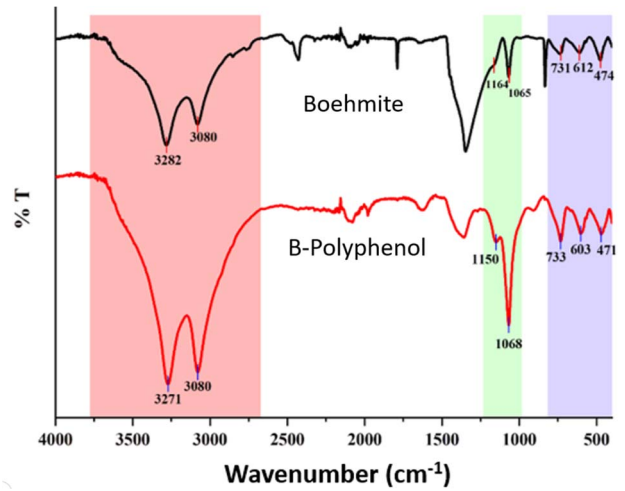

Fig. 5 FTIR spectra of boehmite and B-polyphenol.

polyphenol. It is caused of hydroxide from boehmite was disappeared due to it has bound to polyphenol.[38]

The use of nanomaterials is crucial to study regarding their function and effectiveness as fillers in membrane fabrication. The particle size of the B-polyphenol filler material was analyzed using a particle size analyzer, and the results can be seen in Fig. 4. In Fig. 4, it is evident that the average particle size of the synthesized B-polyphenol is 9.46 nm. Based on the tests using PSA, it is confirmed that the obtained material has a nanoscale size.

The results of the polyphenol compound coating on the boehmite nanomaterial were studied through characterization using FTIR. The FTIR spectrum results can be seen in Fig. 5. The absorption band at 1068 cm^{-1} and the shoulder at 1150 cm^{-1} in the B-polyphenol spectrum indicate the presence of Si–O stretching vibration.[39] This Si–O bond shows that the synthesis of B-polyphenol using the coupling agent CPTES has been successfully carried out. The increase in the width and intensity of the peaks at above 3000 cm^{-1} indicates the formation of hydrogen bonds, confirming that the coating of polyphenol compounds onto the boehmite nanomaterial has been successfully achieved.[26]

Characterization of MMM PES/B-polyphenol

The FTIR characterization aims to assess the success of incorporating the B-polyphenol nanofiller into the membrane. The FTIR results for each membrane can be seen in Fig. 6. The

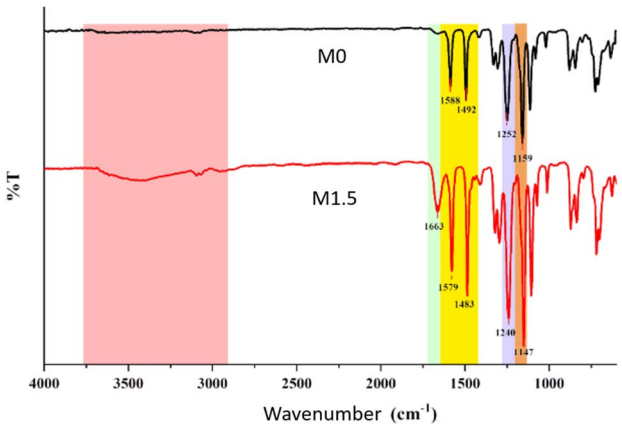

Fig. 6 FTIR spectra of MMM PES/B-polyphenol M0 and M1.5.

absorption band at a wavenumber of 1660 cm^{-1} in the M1.5 spectrum indicates the presence of stretching vibrations in the carbonyl (C=O) bonds originating from the polyphenol compounds integrated into the membrane matrix.[40] The increase in intensity and width of the peaks at wavenumbers greater than 3000 cm^{-1} in the M1.5 spectrum suggests the presence of –OH groups from B-polyphenol. This increase in intensity and peak width indicates that the addition of the nanofiller to the membrane has been successfully accomplished.

The observations using SEM were conducted to compare the surface morphology between membranes M0 (neat) and M1.5. The SEM analysis results can be seen in Fig. 7.

The addition of the nanofiller can lead to a removal in the skin layer thickness of the membrane due to the increased exchange rate between the solvent and non-solvent during the phase inversion occurring during membrane fabrication.[41] Fig. 7 also shows the presence of macropores that have formed. The formation of these macropores may be attributed to the addition of vinyl groups from the poring agent, which possess hydrophilic properties.[42] Similar findings were reported by Eskikaya *et al.* (2024), indicating that the inclusion of nanoparticles in the membrane matrix also leads to an increase in pore size on the membrane surface.[43]

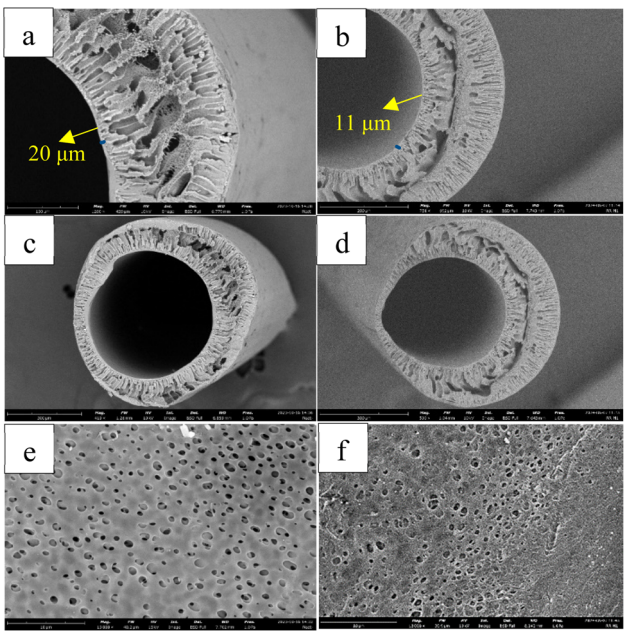

Fig. 7 SEM image of MMM PES/B-polyphenol M0 (a, c and e) and M1.5 (b, d and f).

Table 1 Tensile strength test result of MMM PES/B-polyphenol M0 and M1.5

Membrane	Stress (MPa)	Strain	Modulus Young (MPa)
M0	3.138	0.087	36.07
M1.5	3.435	0.064	53.67

Testing the mechanical properties of a membrane is conducted to study its resistance to external forces. In this tensile strength test, membrane M0 (neat) is used as the control membrane, while membrane M1.5 is selected as the membrane with the best Cr(VI) removal capability. The results of the tensile strength test can be observed in Table 1. It can be seen from Table 1 that the addition of the B-polyphenol filler increases the tensile strength of the fabricated membrane. The modification with B-polyphenol enhances the mechanical properties of the membrane due to the influence of the B-polyphenol distribution within the membrane polymer and the hydrogen bonds formed between B-polyphenol and the PES polymer.[44] However, the strain value of membrane M0 is 26.4% higher than that of membrane M1.5. This could be attributed to the more porous structure of M1.5 compared to M0.[45] Based on Table 1, it is evident that the addition of the B-polyphenol nanofiller increases the Young's modulus value of the membrane, reaching up to 53.67 MPa. A higher Young's modulus value indicates that the material is stiffer, meaning the membrane will be more resistant to elastic deformation when subjected to load or stress.

Porosity test is conducted using the dry–wet weight method, which compares the dry and wet weights of a membrane. The results of the porosity measurements from the fabricated membranes can be seen in Fig. 8. Fig. 8 shows that the porosity of the membranes increases with the addition of the B-polyphenol nanofiller. The incorporation of the nanofiller can lead to increased insolubility of the membrane in non-solvent solutions during the phase inversion process, resulting in enhanced membrane porosity.[46] However, the porosity value of a membrane does not always correlate directly with its filtration capability, excessively high porosity can cause the membrane structure to be more prone to deformation.[47] Based on the porosity graph of the fabricated membranes, it is observed that porosity decreases in membrane M2, which is attributed to the agglomeration of the B-polyphenol nanofiller, leading to blockage in the membrane pores and thus affecting its porosity.[26] In addition, a decrease in porosity can also be caused by the density of the pore structure due to the addition of excessive nanofillers.[48]

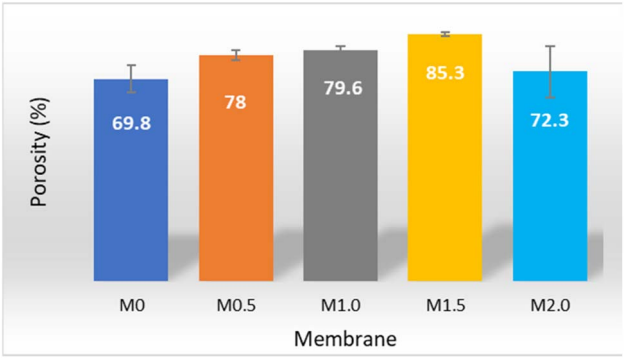

Fig. 8 Porosity graph of M0; M0.5; M1.0; M1.5; and M2.0 membranes.

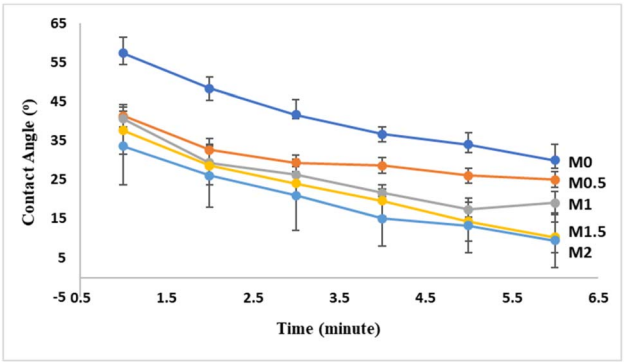

Fig. 9 Hydrophilicity test of M0; M0.5; M1; M1.5; and M2 membranes.

Hydrophilicity test is used to assess the affinity of the fabricated membranes for water molecules. This test involves observing the changes in contact angle between the membrane and water over time. A smaller contact angle indicates a higher hydrophilicity of the membrane. The results of the contact angle measurements between water and the membrane surface are shown in Fig. 9 and 10. As illustrated in Fig. 9 and 10, the hydrophilicity of the MMM PES/B-polyphenol membranes increases with the addition of the B-polyphenol nanofiller. This enhancement in hydrophilicity aligns with the assertion that modifying membranes with the addition of hydrophilic materials can improve their hydrophilicity. The incorporation of the B-polyphenol nanofiller enhances the hydrophilicity of the membrane due to the presence of hydroxyl (–OH) and carbonyl (–C=O) groups on the nanofiller.[41] The magnitude of the contact angle formed is influenced by the ability of water penetration into the membrane surface, while the speed of water penetration is influenced by the hydrophilicity of a membrane. The smaller the contact angle formed indicates the greater the hydrophilicity of the membrane.

The high hydrophilicity of the neat membrane is influenced by the addition of a pore-forming agent polyvinylpyrrolidone (PVP) which also has hydrophilic properties, so that the hydrophilicity of the neat membrane is relatively higher.[49] The addition of B-polyphenol nanofiller can increase the hydrophilicity of the membrane due to the presence of hydroxyl (–OH) and carbonyl (–C=O) groups in the nanofiller. The addition of nanofiller mass causes the contact angle formed between water and the membrane surface to be smaller due to the presence of groups that can form hydrogen bonds between water molecules and the membrane surface.[50] This is in accordance with research conducted by Gao *et al.* (2021),[51] the addition of polyphenol compounds can increase the hydrophilicity of the membrane due to the presence of hydroxyl (–OH) groups in the added phenolic compounds.

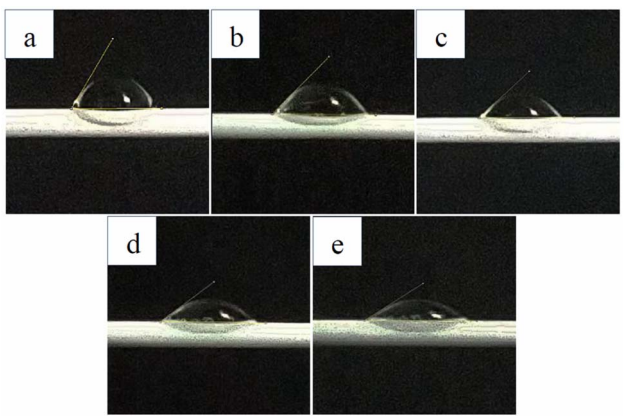

Fig. 10 Contact angle of M0 (a); M0.5 (b); M1 (c); M1.5 (d); and M2 (e).

Water flux

Flux value defines the volume of permeate (mL) that can pass through the membrane per unit area over a unit of time. The results of the water flux are presented in Fig. 11. The water flux increases with the addition of the B-polyphenol nanofiller mass. A 60% increase in flux is observed in the M1.5 membrane compared to the M0 membrane. The increase in water flux can be attributed to the presence of hydroxyl (–OH) groups on the boehmite nanoparticles, which enhance the hydrophilicity of the membrane, leading to higher water flux with the addition of boehmite nanoparticles.[20] Generally, water flux is significantly influenced by hydrophilicity, porosity, and pore size.[20] The larger the pores in the membrane, the greater the amount of permeate that can pass through in a given time, resulting in higher flux values. Fig. 11 also shows a decrease in water flux in the M2 membrane compared to the M1 membrane, which is caused by pore blockage and reduction in pore size due to the agglomeration of the nanofiller.[26]

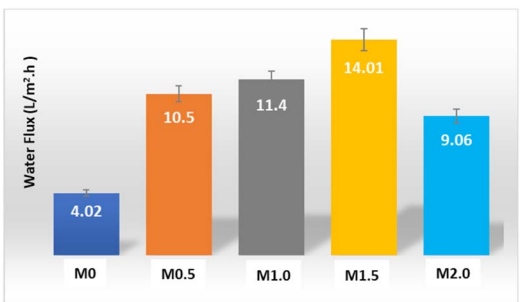

Fig. 11 Water flux of M0; M0.5; M1.0; M1.5; and M2.0 membranes.

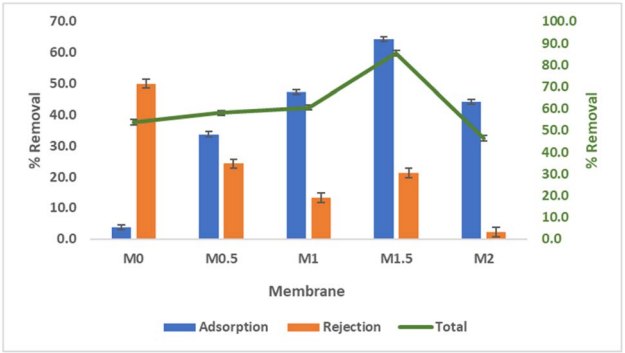

Fig. 12 The influence of B-polyphenol mass on the removal of Cr(VI).

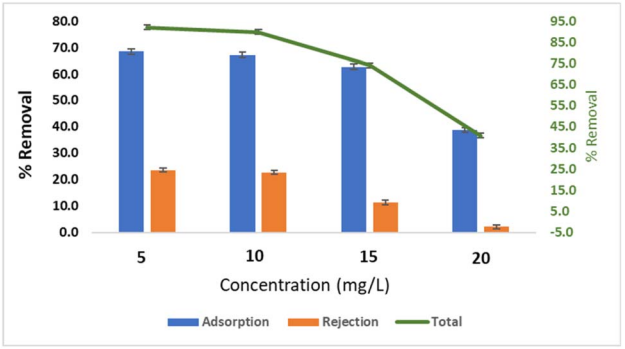

Fig. 14 The influence of feed solution concentration on the removal of Cr(VI).

Cr(VI) removal performance of MMM PES/B-polyphenol

Optimization of B-polyphenol mass. Optimization of mass is essential to determine the maximum amount of filler that can be added to achieve a membrane with the best Cr(VI) removal performance. The results of the optimization of the B-polyphenol filler mass can be seen in Fig. 12. In Fig. 12, there is an observable increase in the percentage removal of Cr(VI) compared to the M0 (neat) membrane, indicating that the addition of B-polyphenol filler to the polymer matrix can enhance the membrane's ability to reduce Cr(VI) levels. The increase is noted from the M0 to M1.5 membranes, followed by a decrease in the M2 membrane. This increase in removal percentage can be attributed to the increased active sites for Cr(VI) binding on the membrane due to the addition of nano-fillers rich in electron-rich groups.[52] In contrast, the decreased absorption capacity in the M2 membrane occurs due to the agglomeration of B-polyphenol within the membrane's pore structure, which hampers the filtration process due to blockage in the membrane pores.[20]

Optimization of the feed solution pH. pH optimization is conducted to determine the feed solution pH value that yields the highest percentage removal of Cr(VI). The results of the pH optimization for the feed solution can be seen in Fig. 13. Fig. 13 shows that in acidic feed solutions, the removal of Cr(VI) is relatively lower compared to that in neutral feed solutions. At acidic pH (pH = 2), Cr(VI) is reduced to the more stable Cr(III) in cationic form.[17,53] The membrane also experiences protonation due to the abundance of H^+ ions in the feed solution. This leads to electrostatic repulsion interactions between the cationic Cr(VI) species and the protonated membrane. The greatest removal of Cr(VI) occurs at pH 6, achieving a removal of 91.11%. This aligns with the observation that at pH 6, boehmite carries a positive charge due to its high point of zero charge (PZC) value. This high PZC value allows boehmite to interact electrostatically with negatively charged species, such as $HCrO_4^-$. At pH 6, Cr(VI) exists primarily as the ionic species $HCrO_4^-$. In basic pH conditions, chromium ions will bind with OH^- in the solution to form $Cr(OH)_3$. The formation of $Cr(OH)_3$ is also evidenced by the presence of solids in the feed solution at basic pH.

Optimization of the feed solution concentration. Optimization of the feed solution concentration is conducted to study the optimal Cr(VI) concentration that can be reduced by the fabricated membrane. The results of the initial feed solution concentration optimization can be seen in Fig. 14. In Fig. 14, it is observed that the percentage removal of Cr(VI) decreases with each increase in the initial concentration of the Cr(VI) feed solution. At an initial concentration of 5 mg L^{-1}, a Cr(VI) removal of 92.12% is achieved. This decrease in percentage removal is due to the MMM PES/B-polyphenol membrane reaching saturation at the active sites for Cr(VI) binding, resulting in a diminished capacity of the membrane to reduce Cr(VI) optimally. This is in line with the research conducted by

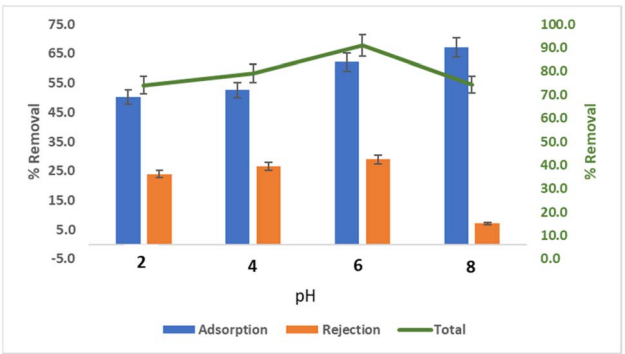

Fig. 13 The influence of pH on the removal of Cr(VI).

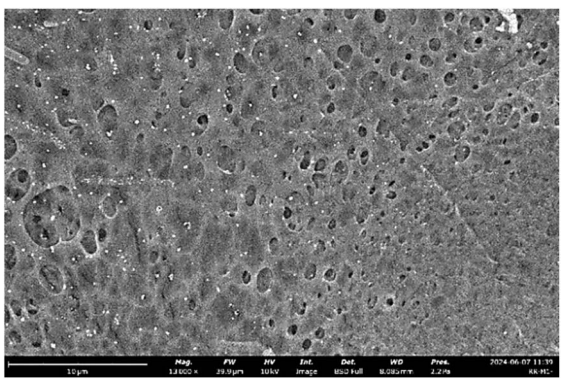

Fig. 15 SEM image of MMM PES/B-polyphenol after Cr(VI) removal.

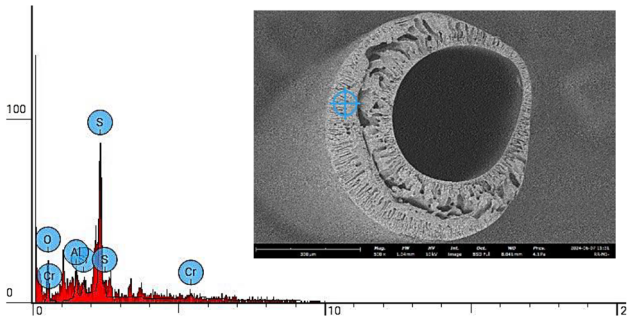

Fig. 16 EDS result of MMM PES/B-polyphenol.

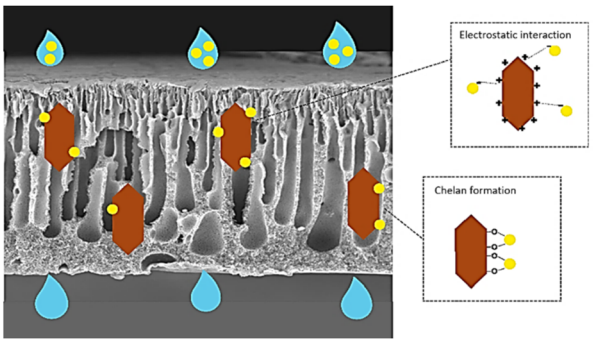

Fig. 17 Illustration of the Cr(VI) removal mechanism.

Table 2 EDS analysis result

Element number	Element symbol	Element name	Atomic conc.	Weight conc.
8	O	Oxygen	21.481	11.800
13	Al	Aluminium	9.396	8.700
14	Si	Silicon	3.214	3.100
16	S	Sulfur	60.307	66.400
24	Cr	Chromium	5.601	10.000

Nie *et al.* (2024), which indicates that a removal in the ability to bind Cr(VI) can occur due to a decrease in the active sites available for binding Cr(VI).[54]

Mechanism of Cr(VI) removal by MMM PES/B-polyphenol

The removal of Cr(VI) by MMM PES/B-polyphenol occurs through several possible mechanisms. The first mechanism involves the adsorption of Cr(VI) in the membrane pores through electrostatic interactions between the metal ions and the membrane surface. Based on the SEM analysis shown in Fig. 15 and EDS shown in Fig. 16, the presence of Cr metal adsorbed within the membrane pores is observed. This is confirmed by EDS, as indicated in Table 2 and Fig. 16, which shows the presence of Cr ions attached to the pores and surface of the membrane. The removal *via* membrane pores is consistent with findings reported by Mahmoud and Mostafa (2023), indicating that metal ions in solution can be separated using a filtration mechanism through the membrane pores.[55]

Based on Fig. 16, the Si element as representative from CPTES, the Al element as representative from boehmite also appear clearly on the MMM PES/B-polyphenol membrane produced. So, from the EDS results, it can be concluded that B-polyphenol particles are embedded in the MMM membrane material which is evenly distributed on the upper, lower and middle surfaces of the membrane.

Another possible mechanism is the binding of Cr(VI) by the –OH groups from the phenolic compounds and the boehmite nanofiller integrated into the membrane. Chemical bonding occurs between the metal ions and the electron-rich groups on the membrane fillers used.[52] The presence of carboxyl (–COOH) and hydroxyl (–OH) groups in the membrane plays a crucial role in the adsorption process of heavy metals.[56] These groups can bind with metal ions in the solution, then forming a chelates. An illustration of the Cr(VI) removal mechanism can be seen in Fig. 17.

Conclusions

Mixed matrix membranes PES/B-polyphenol have good characteristics for Cr(VI) removal. Porosity is formed and PES/B-polyphenol is evenly distributed. The membrane has hydrophilic properties with a water contact angle of less than 90°. The membrane has porosity exceeding 80%. In terms of performance, a water flux value of 14.1 L m^{-2} h^{-1}. Based on tensile strength tests, it was observed that the Young's modulus value of the membrane was 56.67 MPa. The membrane performance test against Cr(VI) obtained a total cleaning result by the membrane of 92.12%. Based on the results obtained, this mixed matrix hollow fiber membrane PES/B-polyphenol has potential to be applied on a larger scale regarding its application to reduce Cr(VI) levels.

Data availability

The data will be made available on request. The data that support the findings of this study are available from the corresponding author upon reasonable request, including: experimental data on the fabrication of the membrane, characterization, performance, and findings on the developed membrane.

Conflicts of interest

The authors declare no conflict of interest.

Acknowledgements

The authors express gratitude to DRPM (Directorate of Research and Community Service, Deputy for Strengthening Research and Development, Ministry of Research and Technology/National Research and Innovation) Indonesia's Research, grant no: 1228/UN3/2024 by Penelitian Tesis Magister (PTM).

References

1 T. Al-Samman, *Mater. Des.*, 2015, **65**, 983–988.
2 M. Nur-E-Alam, M. A. S. Mia, F. Ahmad and M. M. Rahman, *Appl. Water Sci.*, 2020, **10**, 1–22.
3 A. D. Dayan and A. J. Paine, *Hum. Exp. Toxicol.*, 2001, **20**, 439–451.
4 K. Shekhawat, S. Chatterjee and B. Joshi, *Int. J. Adv. Res.*, 2015, **3**, 167.
5 H. Li, Y. Zhang, S. Li, Y. Wang and H. Li, *Environ. Sci. Pollut. Res.*, 2023, **30**, 100466–100476.
6 B. Wionczyk, W. Apostoluk and W. A. Charewicz, *Hydrometallurgy*, 2006, **82**, 83–92.
7 J. Liang, X. Huang, J. Yan, Y. Li, Z. Zhao, Y. Liu, J. Ye and Y. Wei, *Sci. Total Environ.*, 2021, **774**, 145762.
8 J. Valentín-Reyes, R. B. García-Reyes, A. García-González, E. Soto-Regalado and F. Cerino-Córdova, *J. Environ. Manage.*, 2019, **236**, 815–822.
9 L. Liu, Y. Xu, K. Wang, K. Li, L. Xu, J. Wang and J. Wang, *J. Membr. Sci.*, 2019, **584**, 191–201.
10 M. Su, Y. Fang, B. Li, W. Yin, J. Gu, H. Liang, P. Li and J. Wu, *Sci. Total Environ.*, 2019, **647**, 47–56.
11 C. C. Viggi, F. Pagnanelli, A. Cibati, D. Uccelletti, C. Palleschi and L. Toro, *Water Res.*, 2010, **44**, 151–158.
12 Z. Wang, Z. Tan, H. Li, S. Yuan, Y. Zhang and Y. Dong, *J. Cleaner Prod.*, 2022, **339**, 130746.
13 S. P. Dubey, A. D. Dwivedi, M. Sillanpää, H. Lee, Y. N. Kwon and C. Lee, *Chemosphere*, 2017, **169**, 99–106.
14 M. A. Islam, M. J. Angove, D. W. Morton, B. K. Pramanik and M. R. Awual, *J. Environ. Chem. Eng.*, 2020, **8**, 103515.
15 H. Alinezhad, M. Zabihi and D. Kahfroushan, *J. Phys. Chem. Solids*, 2020, **144**, 109515.
16 V. thi Quyen, T. H. Pham, J. Kim, D. M. Thanh, P. Q. Thang, Q. Van Le, S. H. Jung and T. Y. Kim, *Chemosphere*, 2021, **284**, 131312.
17 V. U. Kavitha and B. Kandasubramanian, *SN Appl. Sci.*, 2020, **2**, 1081.
18 N. N. Chauhan, P. Vasava and S. Patel, *Int. J. Creat. Res. Thoughts*, 2020, **8**, 2320–2882.
19 S. Narayanasamy, V. Sundaram, T. Sundaram and D. V. N. Vo, *Environ. Res.*, 2022, **210**, 112902.
20 G. Moradi, S. Zinadini and L. Rajabi, *Chem. Eng. Res. Des.*, 2020, **158**, 148–163.
21 G. T. M. Kadja, E. Dwihermiati, F. Sagita, K. Mukhoibibah, K. Umam, M. Ledyastuti and C. L. Radiman, *Inorg. Chem. Commun.*, 2023, **157**, 111263.
22 Y. Liu, Q. Han, T. Li, J. Hua, F. Liu, Q. Li and G. Deng, *J. Membr. Sci.*, 2020, **595**, 117593.
23 Y. Raharjo, A. F. Ismail, M. H. D. Othman, M. Z. Fahmi, N. Saiful, D. Santoso, M. I. Nugroho, D. Merna, M. D. Arief and R. C. Pratama, *RSC Adv.*, 2023, **13**, 2972–2983.
24 X. Fang, J. Li, X. Li, S. Pan, X. Sun, J. Shen, W. Han, L. Wang and B. Van der Bruggen, *J. Colloid Interface Sci.*, 2017, **505**, 642–652.
25 C. Zhao, J. Xue, F. Ran and S. Sun, *Prog. Mater. Sci.*, 2013, **58**, 76–150.
26 F. Oulad, S. Zinadini, A. A. Zinatizadeh and A. A. Derakhshan, *Chem. Eng. J.*, 2020, **397**, 125105.
27 G. Hazarika and P. G. Ingole, *Mater. Today Chem.*, 2024, **38**, 102109.
28 L. Rajabi and A. A. Derakhshan, *Sci. Adv. Mater.*, 2010, **2**, 163–172.
29 G. Moradi, S. Zinadini and L. Rajabi, *J. Environ. Chem. Eng.*, 2020, **8**, 104431.
30 Y. Raharjo, A. F. Ismail, M. H. D. Othman, M. Z. Fahmi, N. Saiful, D. Santoso, M. I. Nugroho, D. Merna, M. D. Arief and R. C. Pratama, *RSC Adv.*, 2023, **13**, 2972–2983.
31 F. Oulad, S. Zinadini, A. A. Zinatizadeh and A. A. Derakhshan, *Chem. Eng. J.*, 2020, **397**, 125105.
32 A. Esfarjani and M. M. Shokrieh, *Int. J. Adhes. Adhes.*, 2024, **130**, 103604.
33 B. Qiao, T. J. Wang, H. Gao and Y. Jin, *Appl. Surf. Sci.*, 2015, **351**, 646–654.
34 K. M. Hello, A. A. Ibrahim, J. K. Shneine and J. N. Appaturi, *S. Afr. J. Chem. Eng.*, 2018, **25**, 159–168.
35 H. T. He, L. C. Xing, J. S. Zhang and M. Tang, *Energy Explor. Exploit.*, 2016, **34**, 735–745.
36 L. Rajabi and A. A. Derakhshan, *Sci. Adv. Mater.*, 2010, **2**, 163–172.
37 E. Shahed, M. Zabihi and J. R. Shahrouzi, *Chem. Eng. Res. Des.*, 2024, **203**, 321–332.
38 L. A. Kaledin, F. Tepper and T. G. Kaledin, *Int. J. Smart Nano Mater.*, 2016, **7**, 1–21.
39 E. San Andrés, A. Del Prado, F. L. Martínez, I. Mártil, D. Bravo and F. J. López, *J. Appl. Phys.*, 2000, **87**, 1187–1192.
40 Y. Ren, Y. Han, X. Lei, C. Lu, J. Liu, G. Zhang, B. Zhang and Q. Zhang, *Colloids Surf., A*, 2020, **604**, 125279.
41 L. Bai, H. Wu, J. Ding, A. Ding, X. Zhang, N. Ren, G. Li and H. Liang, *Chem. Eng. J.*, 2020, **382**, 122919.
42 H. Mokarizadeh and A. Raisi, *Environ. Technol. Innovation*, 2021, **23**, 101701.
43 O. Eskikaya, R. Kucukosman, S. Ozdemir, M. S. Yalcin, K. Ocakoglu and N. Dizge, *J. Water Process Eng.*, 2024, **57**, 104581.
44 N. A. Johari, N. Yusof and A. F. Ismail, *Mater. Today: Proc.*, 2020, **46**, 1954–1958.
45 N. N. Gumbi, M. Hu, B. B. Mamba, J. Li and E. N. Nxumalo, *J. Membr. Sci.*, 2018, **566**, 288–300.
46 R. A. Milescu, C. R. Mcelroy, T. J. Farmer, P. M. Williams, M. J. Walters, J. H. Clark and Z. Xie, DOI:DOI: **10.1155/2019/9692859**.
47 Y. Feng, E. Shamsaei, C. H. J. Davies and H. Wang, *Mater. Chem. Phys.*, 2015, **167**, 209–218.
48 M. Farjami, A. Moghadassi, V. Vatanpour, S. M. Hosseini and F. Parvizian, *J. Ind. Eng. Chem.*, 2019, **72**, 144–156.
49 N. Arahman, Mukramah, Syawaliah, T. Maimun and M. R. Bilad, *Int. J. GEOMATE*, 2018, **15**, 51–57.
50 L. Bai, H. Wu, J. Ding, A. Ding, X. Zhang, N. Ren, G. Li and H. Liang, *Chem. Eng. J.*, 2020, **382**, 122919.
51 C. Gao, H. Chen, S. Liu, Y. Xing, S. Ji, J. Chen, J. Chen, P. Zou and J. Cai, *Surf. Interfaces*, 2021, **25**, 101301.
52 M. Rajamani and K. Rajendrakumar, *J. Environ. Manage.*, 2019, **244**, 257–264.

53 B. Nechchadi, D. Gallart-Mateu, M. El Krati, M. de la Guardia and S. Tahiri, *Water, Air, Soil Pollut.*, 2022, **233**, 504.
54 Y. Nie, Z. Zhou, C. Zhao, Y. Kong, B. Huang and J. Ma, *J. Water Process Eng.*, 2024, **63**, 105466.
55 A. E. D. Mahmoud and E. Mostafa, *Membranes*, 2023, **13**, 789.
56 B. Shrestha, J. Kour, K. N. Ghimire, B. Shrestha, J. Kour and K. N. Ghimire, *Adv. Chem. Eng. Sci.*, 2016, **6**, 525–540.